






Typical skyrmions versus bimerons: A long-distance competition in ferromagnetic racetracks

A. S. Araújo , R. J. C. Lopes , V. L. Carvalho-Santos, and A. R. Pereira 


Universidade Federal de Viçosa, Departamento de Física, Avenida Peter Henry Rolfs s/n, 36570-000 Viçosa, MG, Brazil

R. L. Silva  and R. C. Silva 

Departamento de Ciências Naturais, Universidade Federal do Espírito Santo, Rodovia Governador Mário Covas, Km 60, 29932-540 São Mateus, ES, Brazil

D. Altbir 

Departamento de Física, CEDENNA, Universidad de Santiago de Chile, USACH, Av. Ecuador 3493, Santiago, Chile

 (Received 26 May 2020; revised 12 August 2020; accepted 24 August 2020; published 8 September 2020)

During the last years, topologically protected collective modes of magnetization have called much attention. Among these, skyrmions and merons have been objects of intense study. In particular, topological skyrmions are structures with an integer skyrmion number Q while merons have a half-integer skyrmion charge q . In this paper, we consider a $Q = 1$ skyrmion, composed of a meron and an antimeron (bimeron), displacing in a ferromagnetic racetrack, disputing a long-distance competition with its more famous counterpart, the typical $Q = 1$ cylindrically symmetrical skyrmion. Both types of topological structures induce a Magnus force, and then they are subject to the skyrmion Hall effect. The influence of the Dzyaloshinskii-Moriya interaction DMI present in certain materials and able to induce DMI skyrmions is also analyzed. Our main aim is to compare the motions (induced by a spin-polarized current) of these objects along with their own specific racetracks. We also investigate some favorable factors which are able to give breath to the competitors, impelling them to remain in the race for longer distances before their annihilation at the racetrack lateral border. An interesting result is that the DMI skyrmion loses this hypothetical race due to its larger rigidity.

DOI: [10.1103/PhysRevB.102.104409](https://doi.org/10.1103/PhysRevB.102.104409)

I. INTRODUCTION

Skyrmions [1] are topologically protected states that have been introduced in the framework of the two-dimensional 2D Heisenberg model (HM) by Belavin and Polyakov [2]. The 2D HM is defined by the Hamiltonian $H = -J \sum_{\langle i,j \rangle} \vec{S}_i \cdot \vec{S}_j$, where $J > 0$ is the ferromagnetic coupling constant, the sum is over nearest-neighbor spins, and the spin field $\vec{S}(\vec{x})$ obeys the constraint $\vec{S}^2(\vec{x}) = S_x^2(\vec{x}) + S_y^2(\vec{x}) + S_z^2(\vec{x}) = S^2$, with S being a constant. Topologically, skyrmions correspond to the mapping of the spin-space sphere $(\sum^{\text{int}})_2$ onto the continuum plane $\vec{r} = (x, y)$ [physical space $(\sum^{\text{phy}})_2$]. Consequently, they are characterized by a skyrmion integer number $Q = \pm 1, \pm 2, \dots$, and have finite energy $E_s = 4\pi JS^2|Q|$, independent of the skyrmion size R , since the continuum limit of the HM, i.e., the $O(3)$ nonlinear σ model, is scale invariant.

Considering the mapping $(\sum^{\text{int}})_2 \rightarrow (\sum^{\text{phy}})_2$, the Belavin-Polyakov skyrmion configurations can have essentially two faces as seen by different perspectives, which depend on the boundary conditions (or stereographic projection). Really, due to the $O(3)$ symmetry, one can look at the situation as follows: for $\vec{S}(\vec{r}) \rightarrow (0, 0, \pm S)$ as $\vec{r} \rightarrow \infty$, one gets the $|Q|$ core configuration [type-I skyrmion, see Fig. 1(a)] while for $\vec{S}(\vec{r}) \rightarrow (\pm S, 0, 0)$ as $r \rightarrow \infty$, one gets the $2|Q|$ core configuration (type-II skyrmion, Figs. 1(b) or 1(c)). For the same Q , both skyrmions (type I and type II) have the same energy. Therefore, we mean that the core occupies a small localized region

in which $S_x^2 + S_y^2 = 0$ and, consequently, $S_z = \pm S$. However, depending on parameters like small anisotropies, external magnetic fields, or others that should favor out-of-plane or in-plane spins, structures similar to type-I or type-II skyrmions, respectively, could be excited in a system. For instance, when a small external magnetic field is applied along the magnetic track, the spins tend to align in plane. After the field is turned off, the tendency of the system is to create type-II skyrmions. On the other hand, if the field is applied along the z direction and it is turned off after some time, the track should host type-I skyrmions. Moreover, magnetic materials with a small easy-plane anisotropy should support excitations very similar to type-II skyrmions. It is important to mention that, in quasi-2D isotropic magnetic materials, skyrmions described above with energy equal to E_s were indirectly detected in experiments using heat-capacity measurements [3] and electron paramagnetic resonance linewidth measurements [4].

In our paper, we consider $Q = \pm 1$ skyrmions since they are energetically favorable. Because type-I skyrmions exhibit great potential to be used in storage and processing-information technologies, much attention has been dedicated to study such a spin texture [5,6]. However, for those applications, some intrinsic difficulties in generating and guiding them along a nanostripe need to be overcome. For instance, to use them in spintronic applications, the main barrier is the inability to move skyrmions straight along applied currents. Indeed, it is well known that type-I skyrmions suffer the

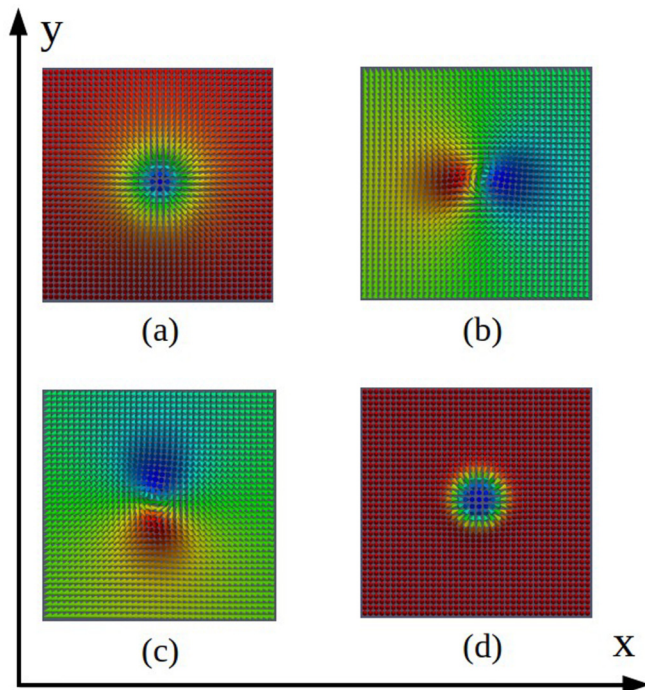


FIG. 1. Spin projection along the z axis, normal to the racetrack plane (x, y), is depicted in color. (a) Type-I skyrmion texture. (b) h bimeron. (c) v bimeron. (d) DMI skyrmion. The current is applied along the x direction and each type of skyrmion runs in its own lane.

effect of the Magnus force, which leads to the skyrmion Hall effect. Among some theoretical propositions to suppress the skyrmion Hall effect, there are possibilities of engineering magnetic materials [7], the formation of coupled skyrmions displacing in bilayer compounds [8–10], and spin-current driven skyrmion dynamics [11]. Based on the above, it should be relevant to analyze the dynamics of topological structures with different shapes along pathways to get more insights to prevail over intrinsic technological difficulties.

In this paper, we give attention to type-II skyrmion textures, also called bimerons [12]. These objects are not cylindrically symmetric [13,14] and may also have important consequences in quantum magnetism. For instance, considering 2D antiferromagnets with general spin S and the case $Q = 1$, the merons [15] forming a double core skyrmion [16] are spin- S spinons [17,18], which appear as essential objects in the search for 2D quantum spin-liquid [19] states of spin half ($S = 1/2$). On the other hand, another kind of bimeron structure may also be found in thin chiral magnetic films [20] induced by nonmagnetic impurities [21], as well as stabilized in confined geometries [22].

The main goal of this paper is to analyze the trajectories of both types of skyrmions described above in ferromagnetic racetracks. In principle, it is shown that if we consider a massless model to describe the dynamics of a bimeron, its trajectory and velocity along a nanotrack would be the same as that predicted for type-I skyrmions. Nevertheless, due to its noncylindrical symmetry, the displacement of bimerons mass-center induces an effective mass which is different from the mass of its type-I skyrmion counterpart. Therefore, it should move in a straight line for longer/shorter distances.

Thus, by means of analytical calculations and micromagnetic simulations, we study type-II skyrmions, focusing on their sensitivity to the Magnus force. The results are compared with the trajectories obtained for type-I skyrmions. Here we have to distinguish two categories of type-I skyrmions, which depend on the specific materials in which they can reside: type-I skyrmions living in ferromagnetic materials with Dzyaloshinskii-Moriya interaction, described by a coupling constant D , added to the Heisenberg Hamiltonian H , and genuine type-I skyrmions which subsist in ferromagnets without Dzyaloshinskii-Moriya interaction (DMI). Although they have very similar shapes, the small and basic contrasts between them may lead to different dynamics. For instance, when the DMI is present, the skyrmion has a more rigid structure and its size (controlled by the ratio D/J) remains practically constant during movement. For racetrack materials with DMI, hereafter the skyrmions will be called DMI skyrmions [see Fig. 1(d)] while type-I skyrmions will be held for the natural counterpart of type-II skyrmions. The configurations of the four structures analyzed here are shown in Fig. 1.

II. THEORETICAL MODEL

Type-II skyrmions or bimerons have two centers in which a meron and an antimeron are positioned. A meron with a winding number $\eta = \pm 1$ and core polarization $P = \pm 1$ has a half-integer topological charge $q = \eta P/2$ (the meron wraps only half of the sphere). Therefore, a pair constituted by a meron ($\eta = 1$) and an antimeron ($\eta = -1$) with the same polarization (for example $P = 1$) has opposite skyrmion numbers adding to zero ($Q = 0$) and, thus, such a pair belongs to the same topological sector as uniform ground states. This object would be then topologically unstable since it can be deformed continuously into a ground state with zero skyrmion number. On the other hand, if a pair has a meron and an antimeron with antiparallel core polarizations, these half-integer structures would have equal skyrmion numbers adding to a total of $+1$ or -1 , belonging to a nontrivial topological sector and thus cannot be deformed continuously into a ground state. It is exactly what occurs with bimerons, which are characterized by a topological invariant (the skyrmion number), defined as [23]

$$Q = \frac{1}{8\pi} \int d^2\vec{x} \epsilon_{ij} \epsilon_{\alpha\beta\delta} n_\alpha \partial_i n_\beta \partial_j n_\gamma, \quad (1)$$

where $\hat{n}(\vec{x}) = \vec{S}/S$ is the unit vector parallel to the local magnetization $\vec{S}(\vec{x})$.

The continuum limit of the 2D-isotropic ferromagnet described by a Hamiltonian H consists in the famous $O(3)$ nonlinear σ model, given by $(J/2) \int d^2\vec{x} (\partial_\nu \vec{S})^2$, $\nu = 1, 2$ and the constraint $\vec{S}^2 = 1$ (without loss of generality, we use an unit spin vector). The explicit static spin configuration of a bimeron can be obtained by using boundary conditions $\vec{S} \rightarrow (1, 0, 0)$ at $\vec{r} \rightarrow \infty$. Then, parametrizing the spin vector $\vec{S}(\vec{r})$ by two scalar fields, the polar and azimuthal angles θ and ϕ , $\vec{S} = (\sin \theta \cos \phi, \sin \theta \sin \phi, \cos \theta)$, this static solution with $Q = 1$ (energy equal to $4\pi J$), size R (merons separated by

a distance R) and mass center localized at the origin can be written as

$$\theta_{2c}^{v(h)} = \arccos\left(\frac{R c_i}{\rho^2 + R^2/4}\right), \quad (2a)$$

$$\phi_{2c}^{v(h)} = \arctan\left(\frac{c_i - R/2}{c_j}\right) - \arctan\left(\frac{c_i + R/2}{c_j}\right), \quad (2b)$$

where $\rho = \sqrt{\zeta x^2 + \xi y^2}$, and $(c_i, c_j) = (x, y)$ and $(c_i, c_j) = (y, x)$ for type-II skyrmions with the cores aligned horizontally (h bimeron) and vertically (v bimeron), respectively. If $\zeta = \xi$, we obtain a regular rigid bimeron in which the two cores are not deformed. If $\zeta \neq \xi$, we obtain a bimeron having an elliptical shape. In Figs. 1(b) and 1(c), we show the vector field of the above described model. In particular, Fig. 1(c) depicts a v bimeron with the cores aligned vertically and $\zeta = \xi = 1$. Of course, there is only one type-II skyrmion but depending on its orientation in relation to the x axis, it manifests as v or h bimerons since this solution is not cylindrically symmetric. The coexistence of different types of skyrmions in the same material is not a trivial possibility since they live in systems with different tendencies for spin arrangements (in plane or out of plane).

Aiming to compare the dynamics of I and II skyrmions, we can describe a $Q = 1$ I-skyrmion solution [Fig. 1(a)] with characteristic radius R , energy equal to $4\pi J$, and placed at $(0,0)$, as

$$\theta_{1c} = \arccos\left(\frac{R^2 - \rho^2}{R^2 + \rho^2}\right), \quad \phi_{1c} = \arctan\left(\frac{y}{x} + c\right), \quad (3)$$

where c is an arbitrary constant. In particular, $c = 0$ and $c = \pi/2$ lead to skyrmions with Néel and Bloch characteristics respectively. For the isotropic HM, such c does not have any influence in our calculations. When DMI is taken into account, Néel and Bloch skyrmions should exist in different materials due to the break of the inversion symmetry. However, these differences do not have an influence on dynamics results investigated here and, therefore, we use only the Néel skyrmion.

Micromagnetic simulations are performed to study the stabilization and dynamics of these skyrmion structures. First, we have stabilized the bimeron in a racetrack composed by an isotropic Heisenberg ferromagnetic material at zero temperature by relaxation and using the solutions of the $O(3)$ nonlinear σ model given by expressions Eqs. (2). The investigated racetrack has a width (distance between the upper and lower lateral borders) equal to $L_y = 80a$ and length $L_x = 300a$, where a is the lattice parameter. The calculations consider periodic boundary conditions along the x direction and open boundary condition along the y direction. The bimeron was stabilized with the following parameters: $J = 1$ and $R = 4a$. Similar parameters are also used for type-I skyrmions [Fig. 1(a)]. The tracks are organized in parallel to simulate a hypothetical race between the I and II skyrmions. Since we are studying four structures (I skyrmion, DMI skyrmion, h bimeron, and v bimeron), our imaginary running track is constituted by four lanes, each one made by a ferromagnetic material with characteristics able to support its resident competitor.

In the simulations, for stabilizing a bimeron in the HM, it is sufficient to introduce in the track its configuration given by

Eqs. (2) and subsequently apply a spin-polarized current. So, the bimeron texture relaxes, adjusting its configuration inside the system. The same scheme is valid for the I skyrmion by using the solution given by Eq. (3). Fourth-order Runge-Kutta method is then employed to compute the dynamics of the magnetic moment, \vec{S}_i , by solving the the Landau-Lifshitz-Gilbert LLG equation [24,25],

$$\frac{\partial \vec{S}_i}{\partial t} = -\gamma \vec{S}_i \times \hat{H}_{\text{eff}}^i + \alpha \vec{S}_i \times \frac{\partial \vec{S}_i}{\partial t}, \quad (4)$$

where γ is the gyromagnetic ratio, $\hat{H}_{\text{eff}}^i = -\frac{1}{\mu_s} \frac{\partial \mathcal{H}}{\partial \vec{S}_i}$ is the net effective magnetic field on each spin, and α is the Gilbert damping coefficient. The spin-polarized current is introduced by using the Berger spin-transfer torque [26]:

$$\vec{\tau}_B = p(\vec{j} \cdot \nabla) \vec{S}, \quad (5)$$

and

$$\vec{\tau}_{B\beta} = p\beta \vec{S} \times (\vec{j} \cdot \nabla) \vec{S}, \quad (6)$$

where Eqs. (5) and (6) are the adiabatic and nonadiabatic torques, respectively. Here p is the spin polarization of the electric current density \vec{j} , while the β parameter characterizes its relative strength to the Berger's torque [Eq. (5)].

III. RESULTS

After stabilizing the skyrmions, we have performed micromagnetic simulations to obtain their mass center position as a function of time for four configurations: (i) a DMI skyrmion; (ii) a I skyrmion; (iii) a v bimeron; and (iv) a h bimeron. Here, the the concept of mass center is directly connected to the geometric center of the topological object, being more useful for the noncylindrically symmetric type-II skyrmions. Before presenting the main results, we have to say something about the particularities of DMI structures. Specifically, different from I and II skyrmions, DMI skyrmions demand extra parameters and factors to be stabilized in a magnetic compound, such as the coupling D and the presence of an external magnetic field along the direction perpendicular to the magnetic plane. Instead of using the field, we stabilize this kind of structure by a small easy-axis anisotropy $k_z/J = 0.11$ (with $J = 1$). In addition, we use $D/J = 0.26$ for the Dzyaloshinskii-Moriya coupling constant. These factors convert DMI-skyrmion configurations in rigid structures, much more inflexible than the other skyrmions investigated here. Indeed, DMI structures are heavier than the other skyrmions and their size does not suffer significant variation during their motions as will be discussed below. This hardness is not expected for I and II skyrmions, since they are described only by a Heisenberg Hamiltonian. As a consequence, their sizes may suffer some fluctuations during their motion, mainly when the spin current is initially applied. Further, at first sight, because the II skyrmion has two merons with opposite winding numbers, one may expect that the meron tends to suffer the Magnus force impelling it to, let's say, the upper border, while its counterpart antimeron tends to go to the opposite side, i.e., the lower border [see, for instance, Fig. 1(c)]. Nevertheless, the type-II skyrmion as a whole has a topological number $Q = 1$ and, therefore, it tends to suffer the Magnus force, similar to what happens

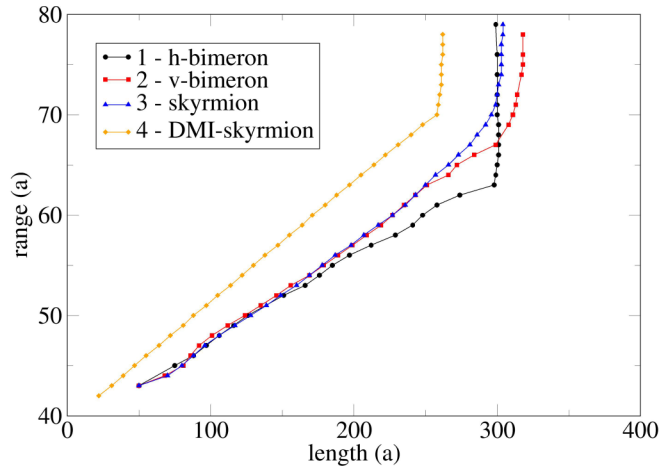


FIG. 2. Trajectories described by the skyrmions (all with $R = 4a$ during their motions in a racetrack with width $L_y = 80a$ and length $L_x = 300a$). Black, red, and blue lines depict the trajectories of the h bimeron, v bimeron, and I skyrmion, respectively. Orange line depicts the trajectory of DMI skyrmion. In a hypothetical race among these objects, the h bimeron would be the winner.

to I skyrmions (all that depends on $q = \eta P/2$; both merons of the bimeron have positive charge $q = 1/2$, moving in the same direction). In other words, the total Magnus force on the structure as a whole is not zero. Therefore, the bimeron mass center moves along the racetrack, suffering the skyrmion Hall effect. The results obtained here confirm this statement. In Fig. 2, we present the respective trajectories followed by the four types of structures during their motions. First, we notice that the deviation from a straight trajectory of a DMI skyrmion (orange line) is greater than all the other ones. That is, if the DMI-skyrmion center starts its motion at the same point of the other structures, it reaches the y border at a smaller position along the x axis (In this paper, we do not discuss the fact that DMI may introduce an extra spin twist in the edge). Additionally, it can be observed that h bimerons suffer a smaller deviation due to the skyrmion Hall effect. Indeed, considering the three skyrmions in materials without DMI, it can be observed that, until the position $x = 250a$, the h bimeron occupies a lower position in the y axis when compared to the v bimeron and I skyrmion. Additionally, the trajectories of II skyrmions are longer than that of the usual type-I skyrmions. On the other hand, since II skyrmions contain two centers, their movements must not occur, keeping a rigid structure, as shown in Ref. [14]. Indeed, the skyrmion may rotate slightly around its mass center and the two merons could have small vibrations during this process. This makes the II skyrmions displace faster along the y direction when they are near the border of the stripe and they are annihilated almost at the same time as the I skyrmion is at the track border (see Fig. 3 and the movies available as Supplemental Material [27]).

To understand the above described results, we will make use of an analytical model, assuming that skyrmions are rigid structures. This assumption is suitable for DMI skyrmions and applies only in a first approximation for the Belavin-Polyakov configurations also treated here. Indeed, for an infinite system, if only exchange interaction is considered, the energy of the

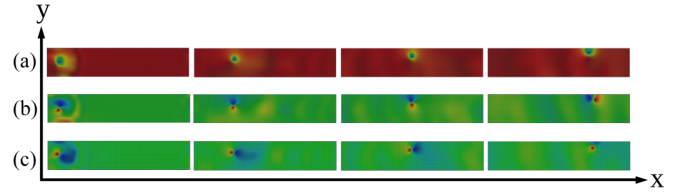


FIG. 3. Snapshots for four subsequent times of the investigated skyrmions in their appropriated tracks during a hypothetical race. Here, it is shown only racetracks made of ferromagnetic materials without DMI; a , b , and c present the evolution of the dynamics of I skyrmion, v bimeron, and h bimeron, respectively.

II skyrmions is independent of the distance R between the meron and the antimeron centers. The same is valid for type-I skyrmions. In this context, the dynamical description of the merons motion can be given by an analytical model neglecting dynamical deformations of the II skyrmions in such a way that the LLG equation can be reduced to the Thiele equation [28], written as

$$\mathcal{M}\dot{\mathbf{v}}(t) + g\hat{z} \times (\mathbf{v}(t) - \mathbf{v}_s) + \mathcal{D}(\alpha\mathbf{v}(t) - \beta\mathbf{v}_s) = \mathbf{F}, \quad (7)$$

where the first contribution consists of an analogous to Newton's second law, with \mathcal{M} being the effective mass of the collective mode of magnetization, with the mass matrix given by

$$\mathcal{M}^{ij} = \frac{1}{\alpha\gamma^2} \int d^2x (\partial^i \tilde{\mathbf{n}} \cdot \partial^j \tilde{\mathbf{n}}). \quad (8)$$

The second term in the Thiele equation describes the Magnus force exerted by the magnetic texture in the collective mode of the magnetization, which displaces with velocity \mathbf{v}_j under the action of the spin current, whose spin velocity parallel to the spin current is \mathbf{v}_s . Here, $g\hat{z}$ is the gyrovector, formally defined as $g = 4\pi Q$, where Q is defined in Eq. (1). The third contribution in Eq. (7) consists of a dissipative force, with \mathcal{D} being the dissipative dyadic, given by $D^{ij} = \alpha\gamma^2 \mathcal{M}^{ij}$. If we consider the parametrization described by Eqs. (2) and (3), with $\zeta = \xi = 1$, the effective mass of I and II skyrmions are the same, given by $\mathcal{M}_s^{11} = \mathcal{M}_s^{22} \equiv \mathcal{M}_s = 8\pi b (\alpha\gamma^2 \sqrt{R^2 + 4b^2})^{-1}$ and $\mathcal{M}_s^{12} = \mathcal{M}_s^{21} = 0$, where $2b = L_y$ is the width of the track and we have considered that $L_y \gg R$. Under these assumptions, the spatial coordinates of all skyrmion structures are obtained from the solution of Eq. (7), evaluated as

$$x(t) = \frac{g^2 v_s}{g^2 + \alpha^2 \mathcal{D}_s^2} t, \quad y(t) = \frac{g \mathcal{D}_s v_s}{g^2 + \alpha^2 \mathcal{D}_s^2} \alpha t. \quad (9)$$

After eliminating the parameter t (time), we get the trajectory equation $y(x) = (\mathcal{D}_s \alpha / g) x$. Note that the function $y(x)$ has a linear dependence on x variable with inclination $\Delta = \mathcal{D}_s \alpha / g \propto \mathcal{M}_s$. The trajectory equation $y(x)$ can be directly compared with the simulation results of Fig. 2. Indeed, this figure shows that the trajectory of all skyrmions obeys an approximated linear dependence $y_i(x) = k_i x$ (here, $i = 1, 2, 3, 4$ refers to the different types of skyrmions). However, the linear behavior of the simulation results prevails only up to a certain critical value of the x coordinate (let's say, $x_{i,c}$). This is a critical position for the skyrmion in a racetrack, marking the

point where the interaction skyrmion border becomes strong enough to deform the skyrmion configuration, invalidating the application of our analytical results [extra forces should be considered in Eq. (7)]. Point $(y(x_{i,c}), x_{i,c})$ denotes the position in which the skyrmion i finds its ultimate moments. After $(y(x_{i,c}), x_{i,c})$, the simulations show that the coordinate $y(t)$ increases rapidly with t while $x(t)$ becomes essentially constant ($x(t) \sim x_{i,c}$) (see again Fig. 2).

The analytical trajectory equation obtained above explains the accentuated difference between the trajectories of skyrmions in materials with and without DMI, as seen in Fig. 2. Since the presence of the DMI diminishes the skyrmion radius, the effective mass of the DMI skyrmion is greater than that of the other structures considered here. The initial impact of the spin current on I and II skyrmions increases their sizes appreciably as observed in the simulations, and snapshots of Fig. 3 can give a clear idea about this behavior. Therefore, remembering that $\Delta \propto \mathcal{M}_s$, then the deviation of the DMI-skyrmion trajectory is larger than that of all other skyrmions residing in materials without DMI. Consequently, DMI skyrmion reaches a lower position along the x axis, having a smaller critical x position, confirming simulation results. On the other hand, our analytical calculations imply that all other skyrmions analyzed here, residing in materials without DMI, have equal masses and, consequently, they should follow similar trajectories. A comparison with simulations of Fig. 2 shows that it is true only in certain parts of the skyrmion routes (around halfway, $x \sim 150a$). After that, the h skyrmion, v skyrmion, and I-skyrmion mass-center trajectories disjoint and each skyrmion follows different ways. As a result, their annihilations occur in slightly different x positions.

Trying to explain the small differences that occur in the trajectories of type-I skyrmion and the bimerons (even the initial position of the bimeron affects its route, causing differences in the trajectories of v and h bimerons), we will assume that there are small deformations in the skyrmion profile when they are displacing under the action of a current density [29]. Such a deformation can be represented by $\zeta - \xi \approx \delta$ (see Fig. 4). In this case, by substituting the magnetization profiles given in the set of Eqs. (2) and (3), the mass matrix elements defined in Eq. (8) are given by $\mathcal{M}_d^{12} = \mathcal{M}_d^{21} = 0$ and $\mathcal{M}_d^{11} = \mathcal{M}_d^{22} \equiv \mathcal{M}_d$. Assuming that $|\delta| \ll 1$, we can expand the mass elements of the II skyrmions, neglecting terms on the order of δ^2 . Under these assumptions, we obtain that the mass elements of the v -bimeron configuration are

$$\mathcal{M}_d = \mathcal{M}_s + \frac{4\pi\delta b}{R^2} \left[2\sqrt{\mathcal{A}} \left(\frac{1}{\mathcal{A}} - 2b^2 + 8Ab^4 \right) - \frac{1}{\sqrt{\mathcal{B}}} - \frac{1}{\sqrt{\mathcal{C}}} \right], \quad (10)$$

where $\mathcal{A} = (R^2 + 4b^2)^{-1}$, $\mathcal{B} = (R - 2b)^{-2}$, and $\mathcal{C} = (R + 2b)^{-2}$. The previous equation reveals that if the v bimeron is flattened along the x -axis direction ($\zeta > \xi$), its mass increases, while if the v meron is flattened along the y axis direction ($\zeta < \xi$), its mass decreases. The mass elements for the h bimeron can be also obtained. However, the equations describing them are cumbersome and will be omitted here. In Fig. 5, we show the behavior of \mathcal{M}_d of the h bimeron as a function of δ . It can be observed that the mass elements of the h bimeron behave

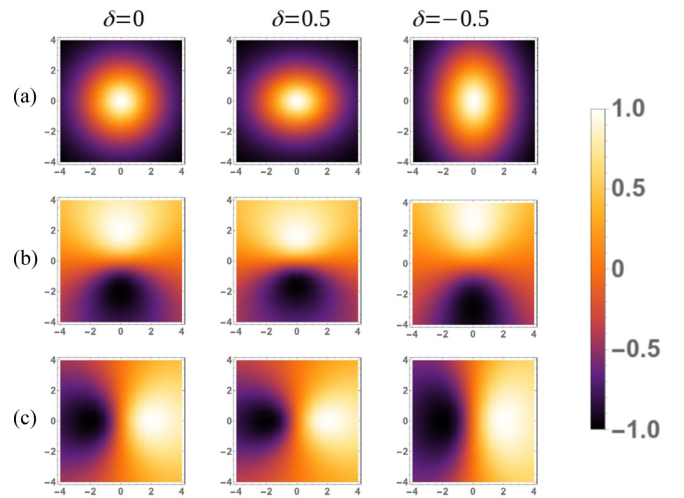


FIG. 4. m_z component of the magnetization of the magnetization of the considered configurations. a , b , and c show respectively the skyrmion, v meron, and h meron for different values of δ .

contrary to the v -bimeron case. That is, for $\delta < 0$ the mass increases when compared to the \mathcal{M}_s , and for $\delta > 0$, the mass decreases. Additionally, the effect of the deformation on the mass is more prominent for h bimerons.

From the above discussion, we are now in a position to explain the results obtained from micromagnetic simulations. Indeed, from the mass-center trajectory equation $y(x) = (D_s \alpha / g)x \propto \mathcal{M}_s x$ [or Eq. (9)], one can observe that the position of the skyrmion depends on its mass in such a way that the larger the mass, the more quickly the skyrmion approaches the lateral border of the racetrack. In principle, the annihilation of the structure at the racetrack lateral border would occur at a smaller x position. In this context, because the v -bimeron mass practically does not change when it deforms, its trajectory should be almost the same as that of the type-I skyrmion. On the other hand, the h bimeron diminishes its mass when it

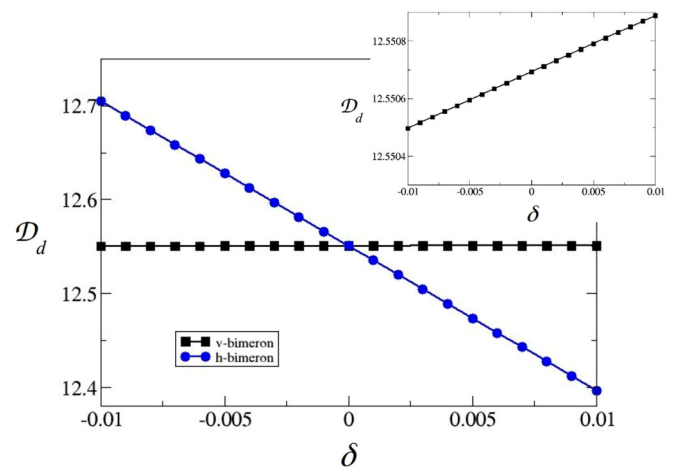


FIG. 5. Behavior of \mathcal{D}_d as a function of δ . Black line (squares) represents the mass element of the v bimeron. Blue line (circles) depicts the mass of a h bimeron. The inset evidences that there is a variation in the v meron mass. In the above figures, we have considered $R = 4$ nm and $b = 40$ nm.

is flattened along the y -axis direction. Nevertheless, because the changes in the skyrmion mass are more pronounced for h bimerons, the trajectory of this structure must have a more pronounced difference as compared with the type I-skyrmion pathway. Such results agree with the simulations. However, when all structures are near the stripe border ($x \sim x_{i,c}$), the deformation along x -axis direction increases the h -bimeron mass and is rapidly destroyed in the stripe border. Because we have considered a model for very small δ , the trajectories analytically obtained are almost superposed, and then a fully realistic model should consider larger deformations. In addition, at $x \sim x_{i,c}$, the skyrmion-border interaction is also important for the skyrmion deformation, changing more drastically the skyrmion trajectories as shown by the simulations.

IV. DISCUSSION AND CONCLUSION

In summary, we have investigated how different skyrmion configurations travel along isotropic ferromagnetic racetracks. Since these skyrmions reside, in general, on different circumstances or materials (for instance, in-plane or out-of-plane

boundary conditions dictate their structures), we have considered a race competition among them in which each skyrmion moves in its own appropriated lane. Since all the objects analyzed here experience the Hall skyrmion effect, they inevitably will die after running some distance along the racetrack (striking the lateral border). We show that the trajectories of these skyrmions depend on their mass, in such a way that small modifications in the mass may result in an additional last breath, making determined skyrmion to live a bit more in the track. Our results show that a bimeron positioned in the v -bimeron mode is the best long-distance runner since it could go through a little more spatial extension before its annihilation at the lateral border of its racetrack. In spite of the skyrmion-border interaction not being included, the presented theory gives a useful tool to understand the behavior of these different magnetic textures.

ACKNOWLEDGMENTS

The authors would like to thank CAPES—Finance Code 001, CNPq, FAPEMIG, and also the financial support from Financiamento Basal AFB 180001 para Centros Científicos y Tecnológicos de Excelencia.

-
- [1] T. H. R. Skyrme, *Proc. R. Soc. Lond. A* **262**, 237 (1961).
 [2] A. A. Belavin and A. M. Polyakov, *Pis'ma Zh. Eksp. Teor. Fiz.* **22**, 503 (1975); *JETP Lett.* **22**, 245 (1975).
 [3] F. Waldner, *Phys. Rev. Lett.* **65**, 1519 (1990).
 [4] C. E. Zaspel, T. E. Grigereit, and J. E. Drumheller, *Phys. Rev. Lett.* **74**, 4539 (1995).
 [5] X. Z. Yu, Y. Onose, N. Kanazawa, J. H. Park, J. H. Han, Y. Matsui, and Y. Nagaosa, *Nature* **465**, 901 (2010).
 [6] S. Heinze, K. von Bergmann, M. Menzel, J. Brede, A. Kubetzka, R. Wiesendanger, G. Bihlmayer, and S. Blugel, *Nat. Phys.* **7**, 713 (2011).
 [7] D. Toscano, J. P. A. Mendonça, A. L. S. Miranda, C. I. L. de Araujo, F. Sato, P. Z. Coura, and S. A. Leonel, *J. Magn. Mag. Mat.* **504**, 166655 (2020).
 [8] X. Zhang, Y. Zhou, and M. Ezawa, *Nat. Commun.* **7**, 10293 (2016).
 [9] A. Hrabec, J. Sampaio, M. Belmeguenai, I. Gross, R. Weil, S. M. Chérif, A. Stashkevich, V. Jacques, A. Thiaville, and S. Rohart, *Nat. Commun.* **8**, 15765 (2017).
 [10] R. Cacilhas, V. L. Carvalho-Santos, S. Vojkovic, E. B. Carvalho, A. R. Pereira, D. Altbir, and Á. S. Núñez, *Appl. Phys. Lett.* **113**, 212406 (2018).
 [11] B. Göbel, A. Mook, J. Henk, and I. Mertig, *Phys. Rev. B* **99**, 020405(R) (2019).
 [12] X. Zhang, J. Xia, L. Shen, M. Ezawa, O. A. Tretiakov, G. Zhao, X. Liu, and Y. Zhou, *Phys. Rev. B* **101**, 144435 (2020).
 [13] O. A. Tretiakov and O. Tchernyshyov, *Phys. Rev. B* **75**, 012408 (2007).
 [14] M. A. Amaral, R. L. Silva, A. R. Pereira, and W. A. Moura-Melo, *J. Magn. Magn. Mater.* **321**, 3360 (2009).
 [15] D. G. Gross, *Nucl. Phys. B* **132**, 439 (1978).
 [16] R. L. Fernandes, R. J. C. Lopes, and A. R. Pereira, *Sol. State Commun.* **290**, 55 (2019).
 [17] G. Baskaran, *Phys. Rev. B* **68**, 212409 (2003).
 [18] A. R. Moura, A. R. Pereira, and A. S. T. Pires, *Phys. Rev. B* **75**, 014431 (2007).
 [19] P. W. Anderson, *Science* **235**, 1196 (1987).
 [20] M. Ezawa, *Phys. Rev. B* **83**, 100408(R) (2011).
 [21] R. L. Silva, L. D. Secchin, W. A. Moura-Melo, A. R. Pereira, and R. L. Stamps, *Phys. Rev. B* **89**, 054434 (2014).
 [22] I. A. Iakovlev, O. M. Sotnikov, and V. V. Mazurenko, *Phys. Rev. B* **97**, 184415 (2018).
 [23] R. Rajaraman, *Solitons and Instantons* (North-Holland, Amsterdam, 1984).
 [24] L. Landau and E. Lifshitz, *Phys. Z. Sowjetunion* **8**, 153 (1935).
 [25] T. L. Gilbert, *Phys. Rev.* **100**, 1243 (1955).
 [26] L. Berger, *Phys. Rev. B* **54**, 9353 (1996); *J. Appl. Phys.* **90**, 4632 (2001).
 [27] See Supplemental Material at <http://link.aps.org/supplemental/10.1103/PhysRevB.102.104409> for the video files in the online version of this paper. All movies show the long race between the considered excitations along the racetrack. We have used open boundary conditions along the vertical direction and periodic boundary condition in the horizontal direction. In movie 1 (mv1.mp4), we present the results of the race of a Belavin-Poliakov skyrmion in an isotropic Heisenberg ferromagnet. Movie 2 (mv2.mp4) and movie 3 (mv3.mp4) show the results for the h and v bimerons, respectively. Here, the racetrack is, again, an isotropic Heisenberg ferromagnet. Movie 4 (mv4.mp4) presents the numerical results for a racetrack with the Dzyaloshinskii-Moriya interaction. We reinforce that all excitations start their movement from the same position of the racetrack.
 [28] A. A. Thiele, *Phys. Rev. Lett.* **30**, 230 (1973).
 [29] R. E. Troncoso, and Á. S. Núñez, *Ann. Phys.* **351**, 850 (2014).